Study of Heterogeneous Nucleation of Eutectic Si in High-Purity Al-Si Alloys with Sr Addition

MUHAMMAD ZARIF, BRIAN MCKAY, and PETER SCHUMACHER

Al-5 wt pct Si master-alloys with controlled Sr and/or P addition/s were produced using super purity Al 99.99 wt pct and Si 99.999 wt pct materials in an arc melter. The master-alloy was melt-spun resulting in the production of thin ribbons. The Al matrix of the ribbons contained entrained Al-Si eutectic droplets that were subsequently investigated. Differential scanning calorimetry, thermodynamic calculations, and transmission electron microscopy techniques were employed to examine the effect of the Sr and P additions on eutectic undercoolings and nucleation phenomenon. Results indicate that, unlike P, Sr does not promote nucleation. Increasing Sr additions depressed the eutectic nucleation temperature. This may be a result of the formation of a Sr phase that could consume or detrimentally affect potent AlP nucleation sites.

DOI: 10.1007/s11661-010-0553-3

I. INTRODUCTION

THE mechanism responsible for the modification of eutectic Si in Al-Si alloys has been the subject of scientific interest for a long time, since the original patent describing the effect of Na in Al-Si alloys was filed by Pacz in 1920.[1] The discovery prompted many studies to examine the effect of the addition of alkali and alkaline earth metals[2–9] on Si nucleation and growth. From this work, it is now believed that nucleation is the dominant influencing factor in the modification process.[10,11] However, nucleation itself is notoriously difficult to study because it is affected by the presence of impurities that act as potent heterogeneous nucleation sites. Turnbull and co-workers[12,13] performed experiments studying homogeneous nucleation that showed that, if a liquid metal is divided into small droplets, then large numbers of the droplets will be considerably undercooled prior to solidifying as they contain fewer impurities.

To study heterogeneous nucleation, Wang and Smith devised a novel entrained droplet technique[14] in which they studied the solidification behavior of Sn droplets solidifying in contact with the Al matrix in an Al-10 wt pct Sn alloy. Chadwick and co-workers[15,16] later demonstrated the effectiveness of the same technique in studying the nucleation of Sn droplets in Al-Sn, Bi-Sn, and Zn-Sn systems. The potential of the technique was recognized and developed by Cantor and co-workers,[10,11,17–19] who employed rapid solidification to produce nanometer size droplets, thereby improving the reproducibility of the undercooling (up to 0.2 K [0.2 °C]). They then used this technique to study the effect of Na and P on Al-Si eutectic undercooling.[10,17] When Na was added to a P-containing melt, silicon nucleated at larger undercoolings. This was caused by the formation of Na_3P that reduced the amount of the potent AlP phase[10,17,20] present.

This AlP phase is believed to be responsible for the Si nucleation. The AlP phase is the major nucleation site for eutectic Si because the crystal structure and lattice parameter of AlP has an excellent match with that of Si.[21] The lattice constants for AlP and Si are 0.542 nm and 0.54306 nm, and the corresponding structure types are B_3 and A4, respectively.[22] Mondolfo[20] reported the effect of sodium poisoning which hindered the nucleation as well as growth of the silicon crystal by removing the AlP compound. Cho *et al.*[23] discussed the poisoning effect of Sr on the AlP compound. They proposed that the intermetallic compound Al_2Si_2Sr consumed the AlP, thus reducing the number of nucleated eutectic grains.

The objective of this article is to investigate in detail the effect of different Sr and/or P addition levels on the eutectic undercooling and microstructure in an Al-5 wt pct Si alloy using the entrained droplet technique. The droplet solidification kinetics were studied by differential scanning calorimetry (DSC); thermodynamic simulation software was applied to determine and verify phase formation, and scanning as well as transmission electron microscopy (SEM and TEM, respectively) were employed to study the microstructure of the solidified droplet.

II. EXPERIMENTAL METHODS

A series of Al-Si and Al-Si-Sr master-alloys, with and without P additions, were manufactured, with

MUHAMMAD ZARIF, Ph.D. Student and Chair of Casting Research, is with the University of Leoben, Leoben, Austria. BRIAN MCKAY, Lecturer, is with BCAST Brunel University, Uxbridge, Middlesex, U.K. PETER SCHUMACHER, Professor and Head of Department at Chair of Casting Research, is with the University of Leoben, and Managing Director, with OGI. Contact e-mail: giesskd@unileoben.ac.at

Manuscript submitted November 20, 2009.
Article published online December 8, 2010

composition as given in Table I, using 4N super purity electrolytically refined Al (Hydro Aluminium High Purity GmbH, Grevenbroich, Germany) as well as 5N and 4N purity Si (Siltronic AG, Burghausen, Germany, and SAG AG, Salzburger, Austria, respectively). The P content in the 4N Al was determined by glow discharge mass spectroscopy at Evans Analytical Group (Tournefeuille, France) and was 0.4 ± 0.08 ppm. For the addition of Sr, an Al-3.59 wt pct Sr prealloy was manufactured, using 4NAl + 99 wt pct Sr (Johnson Matthey Plc, London, U.K.). For the addition of P, an Al-19 wt pctCu-1.4 wt pct P rod (TECHNOLOGICA GmbH, Bad Homburg, Germany) was used. Quantitative chemical data from the alloys produced were obtained using (optical emission spectroscopy) OES-spark analysis.

The ingots were remelted three times, to ensure homogenization, under a 200 mbar Ar atmosphere in an arc melter. In the melt-spinner, alloy charges of ~2.5 to 3 g were remelted in a quartz crucible (1 mm Ø orifice) and ejected (super heat ΔT = 125 K [125 °C], ΔP = 100 mbar) under reduced He (200 mbar) atmosphere onto a Cu wheel rotating with a wheel speed of 15 ms^{-1}, resulting in ribbons ~3 mm wide and ~80 μm thick. The solidification behavior of ribbons of ~5 mg were investigated in the temperature range from 873 K to 673 K (600 °C to 400 °C) at a cooling rate of 10 K/min (10 °C/min) in a power-compensated DSC (Diamond operated with Pyris7; PerkinElmer, Waltham, MA).

For microstructural examination, the ribbons were carefully ground and polished for optical examination (ZEISS Imager; AXIO, Göttingen, Germany). SEM investigations were performed on an ESEM (QUANTA 200; FEI, Eindhoven, Netherlands) equipped with energy dispersive X-rays (EDX) (INCA x-sight; Oxford Instruments, Oxford, U.K.) system. Thin foil specimens for CTEM (Philips CM12, Philips (FEI) Erich Schmidt Institute, Leoben) were prepared on a Fischione twin-jet electropolisher. The samples were electropolished in an electrolyte containing 1/3 parts of HNO_3 and 2/3 parts of methanol at 273 K (0 °C). Scheil simulation using Thermo-calc software with TTAL5 database also was performed to predict the phases present in the alloys and their formation temperatures.

III. RESULTS

A. *Al-Si Ribbon Microstructure*

Optical microscopy (OM) and SEM were used to verify the presence of entrained droplets within the melt-spun ribbons. Figure 1(a) shows the optical micrographs and Figure 1(b) shows the SEM micrographs of as melt-spun ribbon from the super purity Al-5 wt pct Si master alloy. The microstructure consisted of fine equiaxed aluminum grains with Al-Si eutectic droplets present at Al grain boundaries and entrained within the Al grains.

Table I. The Binary and Ternary Alloys with Designated Purity Levels

Alloy Composition	Al, Si, and Sr Purity Designation	P Content (ppm)	Fe Content (ppm)	Sr Content (ppm)
Al-5 wt pct Si	4N Al + 5N Si	Below the detection limit	<5	—
Al-5 wt pct Si	4N Al + 4N Si	of the instrument <2 ppm	<5	—
Al-5 wt pct Si-Sr	4N Al + 5N Si + 2N Sr		<5	50
Al-5 wt pct Si-Sr	4N Al + 4N Si + 2N Sr		<5	50
Al-5 wt pct Si-Sr	4N Al + 4N Si + 2N Sr		<5	100
Al-5 wt pct Si-Sr	4N Al + 4N Si + 2N Sr		<5	200
Al-5 wt pct Si-Sr	4N Al + 4N Si + 2N Sr		<5	1500
Al-5 wt pct Si-Sr	4N Al + 4N Si + 2N Sr		<5	3000

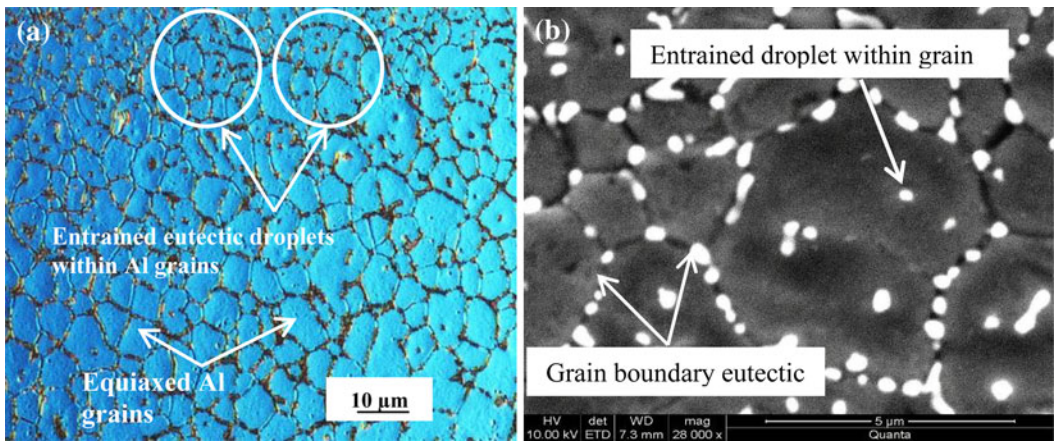

Fig. 1—Distribution of Al-Si eutectic. (*a*) Low-magnification optical micrograph of as melt-spun ribbons, showing Al-Si eutectic present at Al grain boundaries and within Al grains and (*b*) SEM secondary electron image in high-contrast mode.

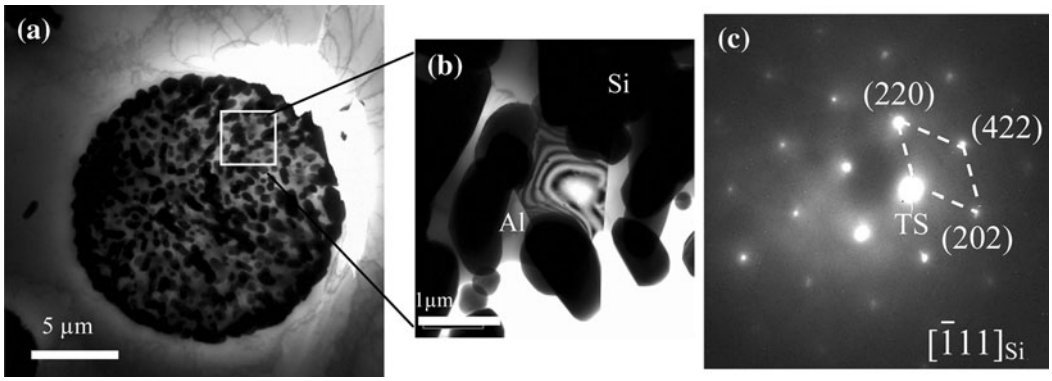

Fig. 2—(*a*) BF TEM image of a eutectic droplet in the super purity Al-5 wt pct Si alloy after DSC, (*b*) at higher magnification, and (*c*) corresponding diffraction pattern.

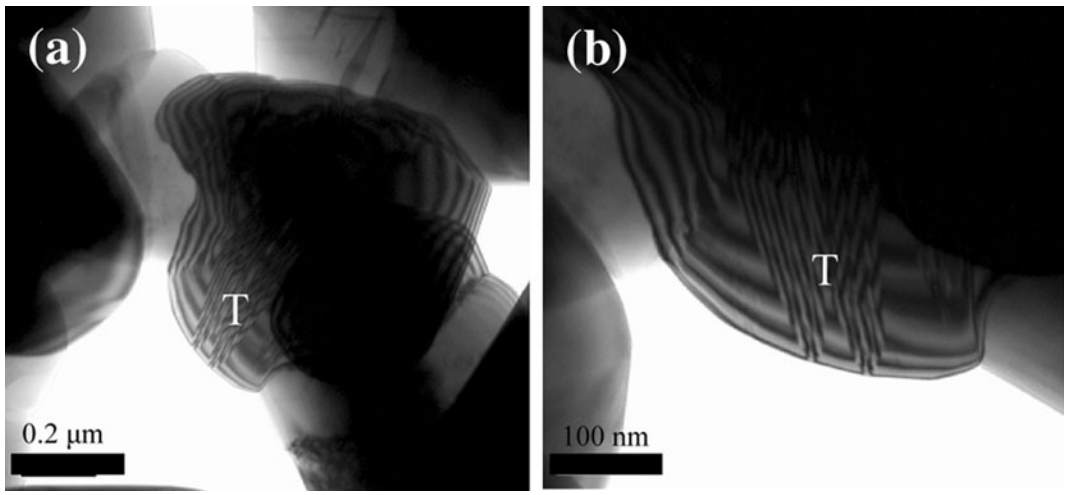

Fig. 3—(*a*) Twinned silicon particle in the eutectic droplet in the as melt-spun super purity Al-5 wt pct Si alloy containing 50 ppm Sr. (*b*) Same silicon particle at higher magnification.

The SEM micrograph was obtained using the Everhart Thornley Detector. This is a standard secondary electron image obtained by applying a positive charge on the scintillator. The selection of the detector mode and the extremely high settings of the brightness and contrast in gray scale resulted in the bright appearance of the Si-containing phases. Figure 2(a) shows a bright-field (BF) TEM image of one such eutectic droplet ~20 to 25 μm in size embedded within the Al matrix. A size distribution of the droplets exists within the melt-spun ribbon. During TEM foil preparation, selective polishing occurs preferentially at larger droplets. As a consequence, in thin regions of the TEM foil, only smaller droplets are observed. As Figure 2(a) shows, the droplet consisted of fine (0.2 to 1.3 μm) silicon particles randomly dispersed between small equiaxed Al grains (Figure 2(b)). A tendency was noted for Si to be observed at the Al matrix interface. Figure 2(c) shows the diffraction pattern taken from a Si particle in the droplet tilted to its $[\bar{1}11]$ zone axis.

Figure 3 shows a twinned silicon particle within a droplet in as melt-spun ribbons (4N + 5N-50 ppm Sr). Twins only are observed when preferentially orientated, and their apparent density seems low as only small areas are investigated here. However, this finding indicates that ΔT was significantly large to force the formation of twins, although the resolution of TEM was not sufficient to observe Sr at re-entrant edges. ΔT is defined on the DSC trace (Figure 4(b)), which is the difference between the onset temperatures of grain boundary and the droplet eutectic ~49 K (49 °C).

B. *DSC Analysis*

DSC investigations were performed to examine the effect of impurities on the eutectic undercooling. Figure 4(a) shows DSC traces obtained from medium and super purity alloys. Each thermogram revealed two distinct solidification exotherms (A and B) at a cooling rate of 10 K/min (10 °C/min). The first sharp exotherm A corresponded to the solidification of grain boundary eutectic, which in both cases occurred at an onset temperature of approximately 847 K (~574 °C) ±0.5, which is 3 K (°C) below the Al-Si equilibrium eutectic temperature documented in the current literature.[24] The smaller exotherm B occurred at onset temperatures of 826 K (~553 °C) ±0.5 and 816 K (~543 °C) ±0.5 for the medium and super purity alloys (*i.e.*, at

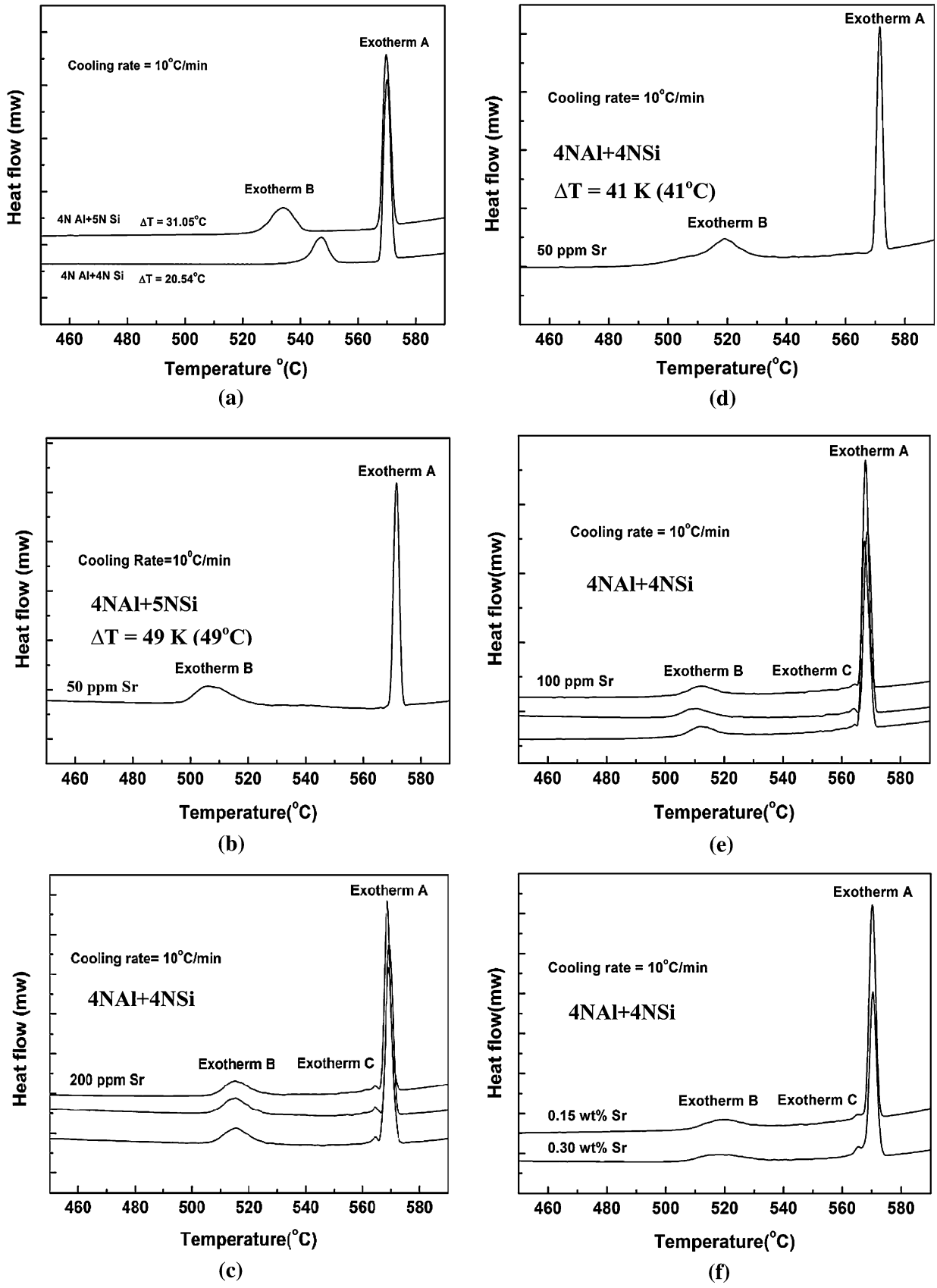

Fig. 4—(*a*) DSC solidification exotherms for medium and super purity binary Al-Si alloys showing the difference of undercooling, and (*b*) through (*f*) DSC traces showing solidification exotherms for ternary Al-Si-Sr alloys with varying Sr addition at a cooling rate of 10 K/min (10 °C/min).

undercoolings of 20 K and 31 K [20 °C and 31 °C], respectively). The reproducibility of the DSC traces was checked for both the medium and the super purity Al-Si alloys and was found to be reproducible to within ±0.5 K (±0.5 °C) at a cooling rate of 10 K/min (10 °C/min). Figures 4(b) through (f) show the effect of different levels of Sr additions on DSC traces.

As Figure 4(d) shows, a Sr addition of only 50 ppm to the medium purity alloy resulted in an increase in the eutectic nucleation undercooling to 41 K (41 °C). With the addition of the same amount of Sr in the super purity alloy, the undercooling increased to 49 K (49 °C) as is shown in Figure 4(b). On increasing the amount of Sr from 50 ppm to 100 ppm or more, a third exothermic peak was observed, exotherm C, which had an onset temperature of 838.5 K (565.5 °C)± 0.5 (Figures 4(c), (e), and (f)). This peak represents the precipitation of an Al_2Si_2Sr intermetallic phase just after (with respect to cooling) the primary solidification exotherm (A), which is the characteristic of an overmodified alloy. Table II gives the measured entrained eutectic droplet undercooling with respect to the effect of the Sr addition. Figure 5(a) shows the DSC solidification exotherm for the super purity Al-Si binary alloy with the addition of 0.5 ppm of phosphorous. The smaller exotherm B occurred with an onset temperature of 832 K (~559 °C). Figure 5(b) presents the DSC trace for the medium purity alloy, which contains 50 ppm Sr and 1 ppm P. The onset temperature for exotherm B was 816 K (543 °C) ±0.5 compared with 806 K (~533 °C) ±0.5 with the addition of 50 ppm Sr only.

Table II. Measurements of Droplet Nucleation Undercooling with the Addition of Sr (P < 2 ppm)

Alloy Name	Additions (Sr)	Undercooling ΔT [K (°C)]
Al-5 wt pct Si super purity	No addition	31 (31)
Al-5 wt pct Si-Sr super purity	50 ppm	49 (49)
Al-5 wt pct Si medium purity	No addition	21 (21)
Al-5 wt pct Si-Sr medium purity	50 ppm	41 (41)

C. *Scheil Simulation*

The alloys liquidus and solidus temperatures, the expected phases, their solid fraction, temperature range, and their approximate percentage volume fraction in the alloys were simulated using the Scheil module from the TCC version of the Thermo-Calc software in conjunction with its TTAL5 database. Figures 6(a) and (b) show the formation temperature and the solidification range of an Al_2Si_2Sr intermetallic phase for two different Sr addition levels. The solidification range and weight fraction of Al_2Si_2Sr increased with the increasing Sr addition.

IV. DISCUSSION

A. *General Microstructure and Undercooling*

The melt-spun Al-5 wt pct Si binary alloys, without any additions, solidified with two exothermic peaks. The sharp exotherm A represents the solidification of grain boundary eutectic, whereas the smaller exotherm B corresponds to the solidification of eutectic droplets within the Al matrix as shown in Figure 4(a). The microstructure of the two-phase eutectic droplet in the super purity alloy as shown in Figure 2(a) revealed that a dominant shell of Si exists at the periphery of the droplet. A simplified estimation of the P content in the droplet, based on equilibrium conditions and zero solubility of P in Al, would result in 40 wt pct eutectic containing all P present (0.4 ppm). This would result in a P content of ~1 ppm in the droplets. This P content is similar to that found by Ho and Cantor[10] and is

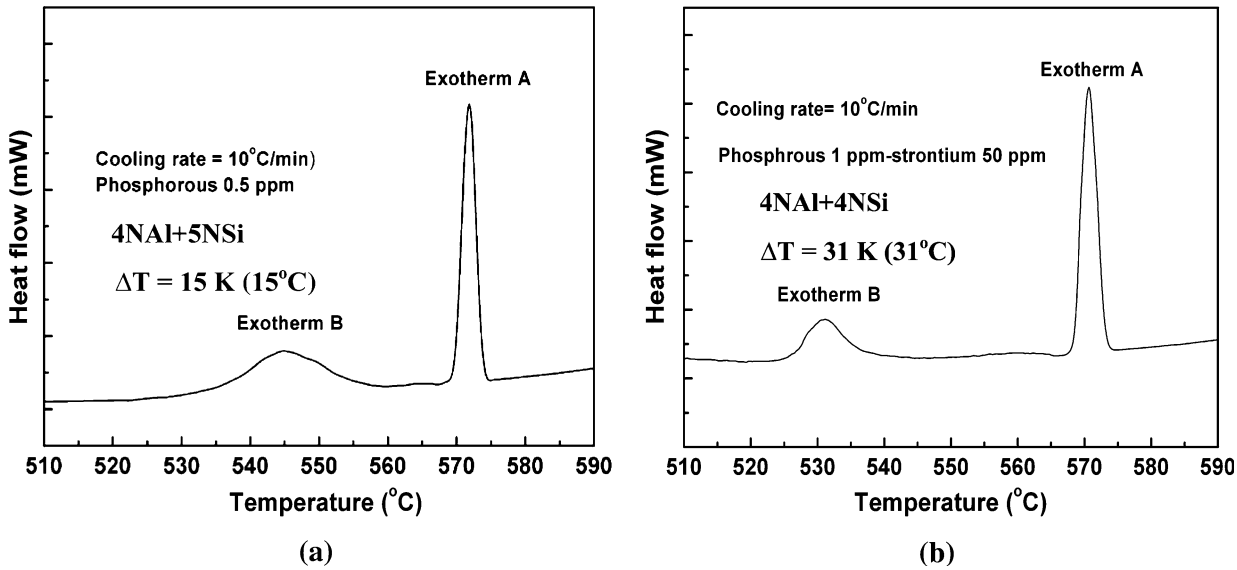

Fig. 5—(*a*) DSC solidification traces for super purity Al-5 wt pct Si-0.5 ppm P and (*b*) medium purity Al-5wt pct Si-50 ppm Sr-1 ppm P.

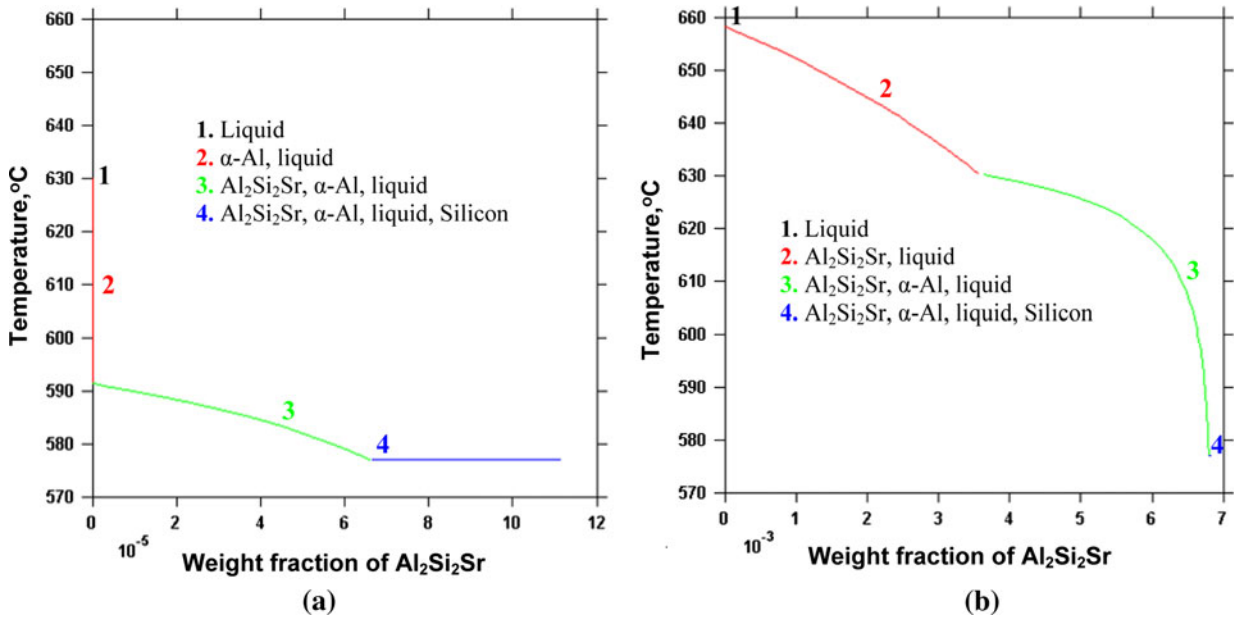

Fig. 6—Scheil simulation performed using TTAL5 database. (*a*) Weight fraction of Al_2Si_2Sr in Al-5wt pct Si-50ppm Sr and (*b*) in Al-5 wt pct Si-0.30 wt pct Sr alloy. The labeled number indicates the solidification range of the solid phase present.

sufficient to observe nucleation of Si on the droplet walls.

It was assumed, as by Ho and Cantor,[10] that a layer of AlP of residual P forms at the interfaces between the Al matrix and the eutectic liquid droplets that heterogeneously nucleate Si. However, no evidence of AlP was found at the interface in this work because of the limited resolution of the TEM employed during this research. The random distribution of the Si particles within the droplets suggested that multiple nucleation[10,17,18] of Si took place, and thus, the curvature of the droplet was significantly bigger than that of the nucleating Si. Therefore, no significant curvature effect was observed.

The smaller undercooling in the medium purity (Figure 4(a)) alloy shows that the presence of impurities has a significant influence on the eutectic nucleation temperature (*i.e.*, the amount of undercooling can depend on the purity of the Al matrix). These results are in good agreement with previous literature.[10,18,25] The addition of only 0.5 ppm of phosphorous in the super purity Al-Si binary alloy caused the smaller exotherm B, as shown in Figure 5(a), to shift toward the sharp exotherm A (*i.e.*, it reduced the amount of undercooling by 16 K [~16 °C]). Published literature[10,21,26] has suggested that the AlP phase is the major nucleation site for Si because of the crystal structure and lattice parameter of AlP, both of which have a good match with that of silicon. Therefore, with a phosphorous addition of only 0.5 ppm, more AlP is available in the entrained droplet for Si nucleation. This result suggests that AlP is a potent and most likely the dominant nucleation site for Si.

B. *Sr Addition and Undercooling*

The Sr addition of 50 ppm to both the super purity and the medium purity Al-5 wt pct Si alloys caused the smaller exotherm (B) to shift to larger undercoolings. The exotherm B occurred with an onset temperature of 806 K (533 °C) ±0.5 and 798 K (525 °C) ±0.5 for the medium and super purity alloys, respectively, as shown in Figures 4(b) and (d). This finding suggests that the Si present within the eutectic droplet nucleates with a larger undercooling, which may be a result of a smaller number of nuclei (possibly a reduction in AlP) available for Si to nucleate on. The onset temperature for the exotherm B remained constant even with the addition of higher levels of Sr in the medium purity alloy, but with the increasing additions, a new peak emerged in the DSC traces, just after (with respect to cooling) exotherm A, as is shown in Figures 4(c), (e), and (f). TEM investigations (Figure 7(a)) revealed the presence of an Al_2Si_2Sr intermetallic phase. This finding was supported by the Thermo-Calc results using the Scheil module (Figures 6(a) and (b)). This intermetallic phase formed (with respect to cooling) before the solidification of the eutectic droplet (*i.e.*, before exotherm B occurred), and therefore, it may be possible that this intermetallic nucleated on the pre-existing AlP particles, thereby reducing the potent Si nucleation sites. Another possible mechanism is related to the formation of Sr_3P_2 compounds. These compounds could act in a similar manner to Na_3P,[17,20,27] which forms in the case of sodium additions. It is possible that the formation of these compounds might reduce the amount of P available in the melt to form AlP. However, these compounds are not observed during TEM investigations.

The argument that the Al_2Si_2Sr intermetallic phase interacted with pre-existing AlP particles can be investigated by examining the DSC thermogram shown in Figure 5(b). The medium purity alloy showed that by keeping the amount of Sr (50 ppm) constant (see Figure 4(d)) and by increasing the addition of P by only

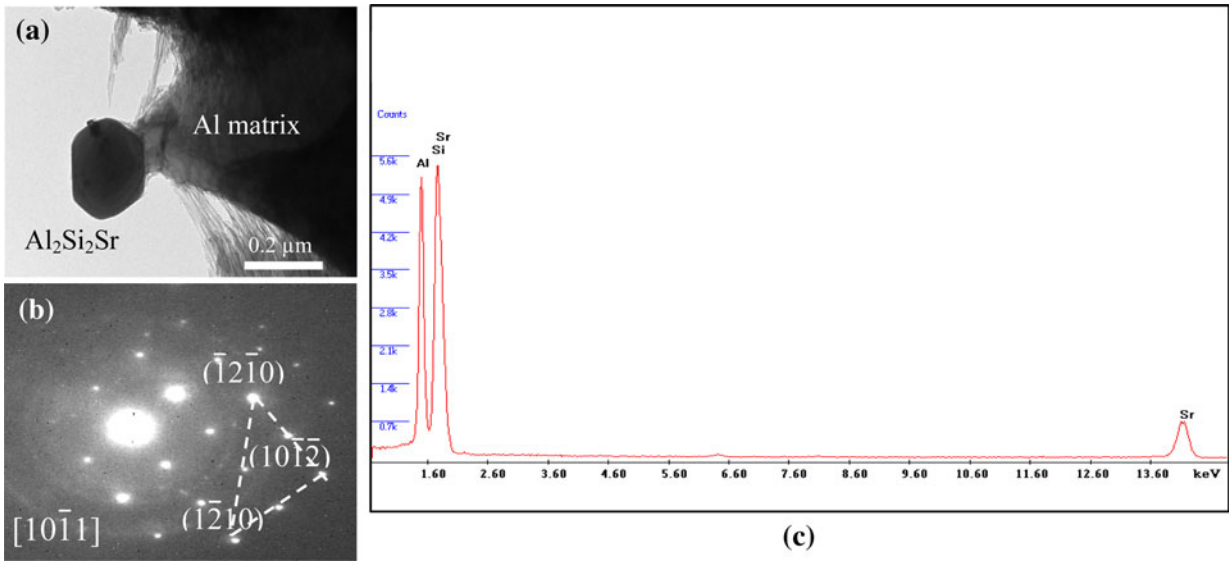

Fig. 7—(*a*) The BF TEM micrograph of the melt spun Al-5 wt pct Si-0.30 wt pct Sr ribbon showing an intermetallic Al_2Si_2Sr particle, (*b*) corresponding SAD pattern, and (*c*) EDX spectrum.

1 ppm, a reduction in the undercooling by approximately 10 K (10 °C) is observed (*i.e.*, exotherm B occurred at an onset temperature of 816 K [543 °C] ±0.5).

From this result, it can be concluded that if the Sr-rich intermetallic nucleates on the AlP compound, some AlP is still available, thereby promoting the eutectic Si nucleation at smaller undercoolings. Crossley and Mondolfo[26] proposed that the addition of modifiers deactivate the AlP, which nucleates eutectic silicon in unmodified alloys. The current results suggest that nucleation is still the dominant factor behind the modification phenomenon. With higher Sr addition levels, Al_2Si_2Sr intermetallic particles formed. This formation will reduce the amount of Sr in the melt and thus its modifying effect.[28] The weight fraction of Al_2Si_2Sr in the two Al-Si-Sr ternary alloys investigated is simulated in Figures 6(a) and (b). These results illustrate that, with increasing the amounts of Sr, the weight fraction of Al_2Si_2Sr intermetallic in the alloy also increases. This results in the precipitation of the Sr intermetallic as a separate peak during solidification. The recent published[23] investigation shows that, if Al_2Si_2Sr precipitates on the pre-existing AlP compound, then the eutectic Si should nucleate at larger undercoolings.

Figure 7(a) shows a BF TEM micrograph of an Al_2Si_2Sr intermetallic particle. The indexed corresponding selected area diffraction (SAD) pattern (shown in Figure 7(b)) revealed a hexagonal $P\bar{3}$ ml (a = 0.4187 nm and c = 0.7427 nm) crystal structure with the particle tilted to its $[10\bar{1}1]$ zone axis. An EDX spectrum from the particle (shown in Figure 7(c)) confirmed the elemental composition. The presence of these intermetallic particles in the Al matrix infer that the AlP phase could interact with these Sr-rich intermetallic particles, thereby causing the Si to nucleate at larger undercoolings.

V. CONCLUSIONS

The entrained droplet technique successfully enables the study of heterogeneous nucleation. The Al-Si eutectic nucleation temperature depended on the purity of the Al matrix. The presence of increasing amounts of impurities within the alloy resulted in the eutectic nucleating at smaller undercoolings. Sr additions are shown not to assist nucleation. Its addition in ppm depressed the eutectic nucleation temperature. This finding may be caused by the formation of an Al_2Si_2Sr intermetallic phase observed in the TEM investigation or by the formation of Sr_3P_2 compounds that were not evident during this study. Scheil simulation indicates that the intermetallic Al_2Si_2Sr phase forms before the eutectic reaction (on cooling). This phase could consume the pre-existing potent AlP particles therefore forcing the eutectic Si to nucleate at larger undercoolings.

ACKNOWLEDGMENTS

The authors would like to thank Professor G. Dehm at the Erich Schmidt Institute, Leoben for access to the TEM facilities and Dr. Rashkova for assistance with TEM imaging. All other experimental work was performed at the Chair of Casting Research, University of Leoben, Austria. In addition, Muhammad Zarif gratefully acknowledges financial support from the Higher Education Commission of Pakistan and managerial support from the ÖAD.

REFERENCES

1. A. Pacz: U.S. Patent 1 387 900, 1921.
2. M.D. Hanna, S.Z. Lu, and A. Hellawell: *Metall. Trans. A*, 1984, vol. 15A, pp. 459–69.

3. S.Z. Lu and A. Hellawell: *Metall. Trans. A*, 1987, vol. 18A, pp. 1721–33.
4. K.F. Kobayashi and L.M. Hogan: *J. Mater. Sci.*, 1985, vol. 20, pp. 1961–75.
5. R.C. Plumb, and J.E. Lewis: *J. Inst. Metals*, 1957-1958, vol. 86, pp. 393–400.
6. V. de L. Davies and J.M. West: *J. Inst. Metals*, 1963-1964, vol. 92, pp. 175–80.
7. A. Knuutinen, K. Nogita, S.D. McDonald, and A.K. Dahl: *J. Light Metals*, 2001, vol. 1, pp. 229–40.
8. A.K. Dahle, K. Nogita, S.D. McDonald, C. Dinnis, and L. Lu: *Mater. Sci. Eng. A*, 2005, vol. 413-4, pp. 243–48.
9. S.D. McDonald, K. Nogita, and A.K. Dahle: *Acta Mater.*, 2004, vol. 52, pp. 4273–80.
10. C.R. Ho and B. Cantor: *Acta Metall. Mater.*, 1995, vol. 43, pp. 3231–46.
11. B. Cantor and K.A.Q. O'Reilly: *Curr. Opin. Solid State Mater. Sci.*, 1997, vol. 2, pp. 318–23.
12. D. Turnbull and J.C. Fisher: *J. Chem. Phys.*, 1949, vol. 17, pp. 71–73.
13. J.C. Fisher, J.H. Hollomon, and D. Turnbull: *J. Appl. Phys.*, 1948, vol. 19, pp. 775–84.
14. C.C. Wang and C.S. Smith: *Trans. AIME*, 1950, vol. 188, pp. 136–38.
15. P.G. Boswell and G.A. Chadwick: *Acta Metall.*, 1980, vol. 28, pp. 209–21.
16. R.T. Southin and G.A. Chadwick: *Acta Metall.*, 1978, vol. 26, pp. 223–31.
17. C.R. Ho and B. Cantor: *J. Mater. Sci.*, 1995, vol. 20, pp. 1912–20.
18. D.L. Zhang and B. Cantor: *Metall. Trans. A*, 1993, vol. 24A, pp. 1195–1204.
19. K.I. Moore, D.L. Zhang, and B. Cantor: *Acta Metall. Mater.*, 1990, vol. 38 (7), pp. 1327–42.
20. L.I. Mondolfo: *Aluminum Alloys: Structure and Properties*, Butterworths Company, London, 1978, pp. 672–82.
21. K. Nogita, S.D. McDonald, K. Tsujimoto, K. Yasuda, and A.K. Dahle: *J. Electron Microsc.*, 2004, vol. 53, pp. 361–69.
22. E.A. Brandes and C.J. Smithells: *Metals Reference Handbook*, 6th ed., Butterworths, London, 1983.
23. Y.H. Cho, H.C. Lee, K. H. Oh, and A.K. Dahle: *Metall. Mater. Trans. A*, 2008, vol. 39A, pp. 2435–48.
24. J.L. Murray and A.J. McAlister: *Bull. Alloy Phase Diagrams*, 1984, vol. 5 (1), pp. 74–84.
25. R.T. Southin: Ph.D. Thesis, Cambridge University, Cambridge, U.K., 1970.
26. P.B. Crosley and L.F. Mondolfo: *AFS Trans.*, 1966, vol. 74, pp. 53–64.
27. B. Cantor: *J. Mater. Sci. Eng. A*, 1997, vol. 20, pp. 151–56.
28. L. Bäckerud, G. Chai, and J. Tamminen: *Solidification Characteristics of Aluminium Alloys Vol. 2 Foundry Alloys*, Amercian Foundry Society, Schaumburg, IL, 1990, p. 37.